6/28/67

TECHNICAL MEMORANDUM

X-495

A COMPILATION OF WIND-TUNNEL HEAT-TRANSFER MEASUREMENTS

ON THE AFTERBODY OF THE PROJECT MERCURY CAPSULE

REENTRY CONFIGURATION

By Kenneth C. Weston and Joanna E. Swanson

Space Task Group
Langley Field, Virginia

NATIONAL AERONAUTICS AND SPACE ADMINISTRATION

WASHINGTON   August 1961

NATIONAL AERONAUTICS AND SPACE ADMINISTRATION

TECHNICAL MEMORANDUM X-495

A COMPILATION OF WIND-TUNNEL HEAT-TRANSFER MEASUREMENTS

ON THE AFTERBODY OF THE PROJECT MERCURY CAPSULE

REENTRY CONFIGURATION[*]

By Kenneth C. Weston and Joanna E. Swanson

SUMMARY

    A compilation of representative wind-tunnel heat-transfer measure-
ments on the afterbody of the Mercury reentry configuration has been
made. It is shown, through comparison, that laminar theory agrees
reasonably well with measurements on the conical section and that
laminar or turbulent theoretical estimates satisfactorily account for
the wide range of wind-tunnel heating measurements which have been
obtained on the cylindrical section. A correlation of the conditions
for the existence of laminar or turbulent cylindrical heat transfer is
presented. Some effects of angle of attack on local windward heat
transfer as well as on circumferential heat transfer are shown. Theory
is also compared with free-flight data from a full-scale Project Mercury
research and development test.

INTRODUCTION

    The prediction of the aerodynamic and thermal characteristics of
wake and rearward-facing afterbody flows has resisted generalized
analytical and experimental treatment for some time. Heat transfer in
separated regions has been studied theoretically by Chapman (ref. 1)
and experimentally by Larson (ref. 2) and others. Powers, Stetson, and
Adams (ref. 3) have correlated the heating in the separated and
reattached regions on the sting supporting a blunt body. Furthermore, a
great deal of ICBM nose cone afterbody data have been obtained, but a
theoretical method for the calculation of the flow and heating over an
arbitrary afterbody is still lacking. Therefore, numerous wind-tunnel

---

[*]Title, Unclassified.

tests have been made over a wide range of conditions to study the heating of the Mercury capsule reentry configuration. This report constitutes an attempt at unifying the experimental results obtained in this program.

SYMBOLS

D	maximum body diameter
h	heat-transfer coefficient
H	stagnation enthalpy
l	surface distance
M	Mach number
p	pressure
q	heat-transfer rate
R	Reynolds number
t	time
α	angle of attack

Subscripts:

1	from stagnation point
2	from heat-shield shoulder
3	from cone-cylinder junction
D	maximum body diameter
sp	at stagnation point
∞	free stream

An asterisk denotes properties evaluated at reference temperature or enthalpy.

AFTERBODY HEAT TRANSFER

Aerodynamic heat-transfer data for the Mercury capsule reentry configuration have been obtained in various wind tunnels of the National Aeronautics and Space Administration and the U.S. Air Force Arnold Engineering Development Center. Table I summarizes the facilities utilized in this program and indicates the wide range of test conditions obtained.

The Mercury capsule reentry configuration is shown in figure 1. The conical, cylindrical, and top canister sections are indicated as well as approximate l_2/D (ratio of surface distance from heat-shield shoulder to maximum body diameter) for various reference locations. All models had a semi-cone angle of $20°$. Slight dimensional variations in addition to scaling existed from model to model, but these variations are believed to cause only small heat-transfer variations. The models were smooth, in general, and did not attempt to simulate the Mercury corrugations or irregularities.

In this report, selected data are compared with flat-plate theory by utilizing a wind-tunnel pressure correlation. A discussion of the methods used to obtain theoretical estimates of local afterbody heat-transfer is given in appendix A. Since it was not feasible to present all available data, references are given from which the remaining published data may be obtained. Emphasis has been placed on the zero angle-of-attack heating with some of the higher angle-of-attack data included for comparison. A comparison of the afterbody reentry data obtained in the flight of a full-scale Project Mercury test vehicle (Big Joe) with similar theoretical calculations is presented in appendix B.

Zero Angle-of-Attack Heating

AEDC-B tunnel.- The distribution of local-to-stagnation-point heat-transfer coefficient obtained in tunnel B of the Von Karman Gas Dynamics Facility at the Arnold Engineering Development Center (hereinafter referred to as AEDC-B tunnel) at a Mach number of 8 and $R_{\infty,D} = 1.6 \times 10^6$ (ref. 4) is shown in figure 2. As there is some doubt concerning the stagnation region heat-transfer coefficients used in reference 4, afterbody measurements presented herein were referenced to estimated stagnation-point values.

Over the forward part of the conical section, the data are found to be in reasonable agreement with laminar estimates obtained as described in appendix A. The rapid rise at the aft part of the conical section may be attributed to thermal conduction from the hotter cylindrical section and/or to transitional boundary-layer conditions in this region.

Measurements on the cylindrical section were found to be an order of magnitude higher than laminar estimates; whereas comparisons made with turbulent estimates agree well with the level of the measurements.

The measurements on the top canister are indicative of the heating in a sheltered separation region and a reattachment region in turbulent flow. No attempt was made to correct the estimates applied immediately aft of the cylindrical section for the obviously separated flow existing there. In the reattachment zone, it is seen that the present calculations underestimate the heating rates by close to 20 percent. It is interesting to note, however, that the same level of heating was measured on the cylinder.

The ratio of midcylinder to stagnation-point heat-transfer coefficient as a function of free-stream Reynolds number is presented in figure 3. Comparison with estimates indicates turbulent or transitional heating above $R_{\infty,D}$ equal to approximately 0.5×10^6 and laminar or transitional below.

Langley Unitary Plan wind tunnel.- Qualitatively similar results to the AEDC-B data were obtained in the Langley Unitary Plan wind tunnel at a Mach number of 4.44 and $R_{\infty,D} = 2.7 \times 10^6$ (ref. 5). These data, shown in figure 4, also indicate reasonable agreement with laminar theory over the forward part of the conical section and with turbulent theory over the forward part of the top canister. Estimates of turbulent heat-transfer coefficients on the cylindrical section exceed measured values by approximately 40 percent.

Langley Mach 5 Blowdown Jet.- A set of unpublished data obtained in the Langley Mach 5 blowdown jet is presented in figure 5. The variation of midcylinder to stagnation-point heat-transfer coefficient ratio with free-stream Reynolds number was compared with laminar and turbulent estimates. Excellent agreement was obtained with turbulent estimates in the range of Reynolds number from 0.5×10^6 to 2.3×10^6. Two points at $R_{\infty,D} = 0.3 \times 10^6$ are evidently laminar, and a single point at the very high Reynolds number of 4.17×10^6 deviates considerably from the turbulent estimates. As discussed in appendix A, the

turbulent estimates have been based on an effective boundary-layer length measured from the cone-cylinder junction. It seems reasonable to assume that with increasing Reynolds number the transition point should move forward from the region of the cone-cylinder junction and result in an increased effective boundary-layer length. As a check of this hypothesis, calculations utilizing the wetted distance from the heat-shield shoulder as the reference length were made. These estimates are shown in figure 5. Since the measured value at $R_{\infty,D} = 4.17 \times 10^6$ falls within the range of estimates based on distance from heat-shield shoulder and cone-cylinder junction, it appears that:

(1) Transition occurs on the cone at this Reynolds number, with a consequent increase in heating there. Unfortunately, there was no instrumentation along the cone and, therefore, the transition point could not be determined.

(2) The calculation procedure described in appendix A should yield conservative results for cylinder heating with increasing Reynolds number.

Langley 11-inch hypersonic tunnel.- Data presented in preceding sections have indicated the existence of laminar heating rates on the forward part of the conical section for $R_{\infty,D}$ equal to or less than 2.7×10^6 and turbulent or transitional heating rates on the cylinder for $R_{\infty,D}$ above approximately 5×10^5. In contrast, it was found in the Langley 11-inch hypersonic tunnel (ref. 6) that laminar flow existed over the entire capsule at $M_{\infty} = 9.6$ and $R_{\infty,D} = 0.2 \times 10^6$. These data are presented in figure 6. The highest heating rates were measured on the top canister section but these are seen to be only 10 percent of the stagnation-point value.

Other Tests.- Representative results from other facilities (obtained from reference 7 and unpublished data) are presented in table II. With the exception of the Ames 10- by 14-inch tunnel data, it is thought that laminar heating rates existed over the entire model in each case. The Ames 10- by 14-inch tunnel data indicated transitional or turbulent flow on the cylindrical section but laminar flow on the cone.

It may be noted that the laminar heating estimates were usually higher than the measurements over the central portion of the conical section in the tests at $\alpha = 0^{\circ}$. This condition is very likely due to separated flow over this region.

Transition at Zero Angle of Attack

The preceding section indicates that reasonable estimates can be made of Mercury afterbody heating rates by using the wind-tunnel pressure correlation provided the condition of the boundary layer is known. Therefore, it is necessary to study the transition problem and determine the conditions under which the boundary layer becomes transitional or turbulent on the Mercury capsule. Unfortunately, no complete determination of transition conditions can be made in a study of wind-tunnel data under the current state of the art because of the number of independent variables affecting the transition problem and the inexact simulation of prototype geometry and flow conditions in the wind tunnel. However, some insight into the problem can be gained by a study of the available data. The condition of the boundary layer at midcylinder, as determined by comparison of heat-transfer measurements at $\alpha = 0^{\circ}$ with theoretical estimates, is summarized in figure 7(a). For each set of conditions, a point, indicative of the type of boundary layer, is plotted in the $M_{\infty} - R_3^*$ plane. (R_3^* is the Reynolds number evaluated at reference enthalpy and based on the distance from the cone-cylinder junction.) Despite the fact that no account has been taken of surface roughness, minor geometry differences, wall-to-local temperature ratio, and the multiplicity of other variables which affect transition, a consistent correlation is obtained of the wind-tunnel midcylinder transitions. Also shown in this figure is a locus of points representing data obtained during the Big Joe flight (ref. 8). The condition of the boundary layer was identified by comparison of measured heating with estimates by using the procedure of appendix A. These measurements are discussed further in appendix B. Results consistent with the wind-tunnel data are shown. Replacing R_3^* by $R_{\infty,D}$ in a similar plot also results in a consistent correlation of the transition condition. (See fig. 7(b).) Figures 7(a) and 7(b) suggest that the boundary-layer condition at midcylinder will not depend strongly on Mach number and will be turbulent for $R_3^* > 10^4$ or $R_{\infty,D} > 0.5 \times 10^6$, and possibly laminar for $R_3^* < 10^3$ or $R_{\infty,D} < 2 \times 10^5$.

A similar analysis of wind-tunnel conical-section heating data suggests that laminar heating may exist at midcone to Reynolds numbers in excess of $R_{\infty,D} = 2 \times 10^6$.

Heat Transfer at Angle of Attack

Because of trim angles of attack or possible capsule oscillations, the effect of angle of attack on afterbody heating is of considerable interest. Figure 8 shows the heat-transfer coefficient distribution (referenced to the stagnation-point heat-transfer coefficient at $\alpha = 0^{\circ}$) along the windward generator at various angles of attack from $\alpha = 0^{\circ}$ to $\alpha = 40^{\circ}$. These data were obtained in the AEDC-B tunnel at $M_{\infty} = 8$ and $R_{\infty,D} = 1.6 \times 10^{6}$.

If reference is made to figure 2, it is seen that turbulent heating existed on the cylindrical section for these conditions at $\alpha = 0^{\circ}$. It therefore appears that the cylindrical-section heating is turbulent at all angles of attack at these conditions. These data indicate a twentyfold increase in conical-section heating from zero incidence to $\alpha = 40^{\circ}$. Heat-transfer coefficients in excess of the stagnation-point values are in evidence on both the cylinder and top canister at $\alpha = 40^{\circ}$.

The conical-section measurements for $\alpha = 10^{\circ}$, 20°, and 30° are replotted in figure 9 for comparison with theoretical laminar estimates. The estimates shown employed the method described in appendix A with two different reference lengths, the distances from the zero angle-of-attack stagnation point and from the heat-shield shoulder. It may be noted that, although the measurements at 10° agree best with the calculations using distance from the zero angle-of-attack stagnation point, the data at the higher angles of attack tend to agree better with the calculations using distance from the heat-shield shoulder as the characteristic dimension. This agreement can be rationalized by noting that the flow stagnation point approaches the heat-shield shoulder closely at the higher angles of attack.

A circumferential distribution of the ratio of midcylinder heat-transfer coefficient to stagnation-point heat-transfer coefficient for angles of attack up to 20° is presented in figure 10. These unpublished data were obtained in the Langley Mach 5 blowdown jet at $M_{\infty} = 4.95$ and $R_{\infty,D} = 2.1 \times 10^{6}$. The cylinder heat-transfer coefficient ratios shown in this figure, as well as in figure 7, are both turbulent and are roughly indicative of the worst condition the cylindrical section of the Mercury capsule should experience in its flight regime. The circumferential extent of high heating rates is seen to be limited to an included angle of about 100° for angles of attack of 10° and 20°.

CONCLUDING REMARKS

Comparisons have been made of Project Mercury afterbody heat-transfer data with flat-plate theories. Reasonable agreement has been obtained in most cases. It has been shown that the wide range of cylindrical heating rates may be attributed to the possibility of both laminar and turbulent flows. A rough correlation of available afterbody data has suggested that cylindrical-section heating for $\alpha = 0^\circ$ will probably be turbulent for $R_3{}^* > 10^4$ or $R_{\infty,D} > 0.5 \times 10^6$ and possibly laminar for $R_3{}^* < 10^3$ or $R_{\infty,D} < 2 \times 10^5$. ($R_3{}^*$ is the Reynolds number evaluated at reference enthalpy and based on surface distance from cone-cylinder junction and $R_{\infty,D}$ is the Reynolds number evaluated for free-stream conditions and based on maximum body diameter.) A similar correlation of wind-tunnel data for the conical section suggests that laminar heating may exist at midcone to Reynolds numbers exceeding $R_{\infty,D} = 2 \times 10^6$. Measurements at high angle of attack have yielded heating rates approaching and, in one instance, exceeding stagnation-point values.

Space Task Group,
    National Aeronautics and Space Administration,
        Langley Field, Va., February 8, 1961.

APPENDIX A

HEAT-TRANSFER ESTIMATES

Pressure Distributions

Analysis of the aerodynamic heating to a body depends strongly on the flow external to the boundary layer and its associated pressure distribution. In the absence of a theoretical method of sufficient accuracy and simplicity for the determination of afterbody pressure distributions for the capsule configuration, an empirical correlation of representative wind-tunnel pressure distributions obtained on the reentry configuration (refs. 4, 6, 7, and 9) has been employed in the present analysis.

This correlation, shown in figure 11, is in terms of the parameter $\frac{p}{p_\infty M_\infty^2}$ which behaves at hypersonic Mach numbers like $\frac{p}{p_{sp}}$. The abscissa of this figure is the surface distance from the heat-shield shoulder nondimensionalized with the maximum body diameter l_2/D. It should be noted that, since the relative length of the cone and cylinder varied slightly with the different models, the values of l_2/D of the cylinder measurements were adjusted to conform to an l_2/D of 0.874 at the cone-cylinder junction. Curves are shown for angles of attack of 0°, 10°, 20°, and 30° for the windward generator.

The parameter $\frac{p}{p_\infty M_\infty^2}$ is reasonably successful in correlating the conical-section pressure measurements into a single band, which for the most part is within the scatter of the data from individual tests. However, this condition is clearly not true on the cylindrical section at $\alpha = 0^\circ$. The inability of the pressure parameter to correlate the zero angle-of-attack cylinder pressure data is evidently due to marked changes in the local flow field. These changes reflect a phenomenon which might be interpreted as varying degrees of flow attachment. An estimate of the effect of Reynolds number on cylindrical pressures at constant Mach number can be obtained by comparing the measurements at $M_\infty = 8$. (See fig. 11.) For the purposes of heat-transfer estimates at $\alpha = 0^\circ$, the variation of the pressure parameter was assumed to be dependent on Reynolds number only. For angles of attack greater than zero, a single curve, faired through all the points at each angle of

attack, was used for all Reynolds numbers.

Heat-Transfer Assumptions

The theoretical heat-transfer calculations presented in figures 2 to 6, and figure 9 are based on isothermal flat-plate calculations utilizing local conditions obtained by assuming an isentropic expansion from stagnation-point conditions to the local pressures obtained from figure 11. Normal shock and local flow properties adjacent to the boundary layer are evaluated by using the tables and charts of reference 10 or references 11 and 12, depending on free-stream conditions. The variable-property approximation of Eckert (ref. 13), known as the reference temperature or reference enthalpy method, was used to evaluate local Stanton numbers from which the local heat-transfer coefficients were obtained.

Laminar heating estimates were based on wetted distance from the stagnation point. In the case of the wind-tunnel calculations for $\alpha = 0^o$, an approximate Mangler transformation (a correction less than 50 percent) was applied to the flat-plate theory on the cone to take into account the geometrical effect on the boundary-layer growth. Turbulent estimates are based on distance from the cone-cylinder junction.

G
8

APPENDIX B

COMPARISON OF THEORETICAL ESTIMATES
WITH BIG JOE FLIGHT DATA

The agreement obtained between wind-tunnel measurements and the theoretical estimates in figures 2 to 6 and 9 immediately suggests a comparison of the Big Joe flight data of reference 8 with the present method discussed in appendix A. Such a comparison is shown for the conical section in figure 12(a) and the cylindrical and top canister sections in figures 12(b) and 12(c), respectively. Heat-transfer rates are shown as a function of time for several stations. All heating rates obtained at a given station are compared to indicate the circumferential variation due to angle of attack. These measurements are compared with theoretical estimates for $\alpha = 0^{\circ}$, since the precise flight orientations are not available for the various instrumentation locations. The effect of angle of attack should, therefore, result in the theoretical prediction being bracketed by the measurements for the several circumferential locations.

Reasonably good agreement was obtained with laminar theory on the conical section, particularly at the forward stations. Comparison of the heat-transfer measurements for the three generators at each station indicates a maximum ratio of heating rates due to angle of attack of about two. This ratio is comparable to the maximum discrepancy between the theoretical estimates and the measurements.

Measurements on the cylinder of the Big Joe capsule configuration are shown in figure 12(b). In this flight, the highest heating rates were measured by thermocouple 12 at midcylinder. Turbulent estimates are shown for this station for angles of attack of 0°, 10°, and 20°. Based on these estimates, a constant angle of attack of approximately 15° is necessary to achieve the peak heating rates measured. Since the thermocouples would sense a time-weighted average heating rate, in the absence of a high trim angle, an oscillation greater than 15° would be required to produce heating equivalent to a constant angle of attack of 15°. Such an amplitude is not compatible with the estimated maximum oscillatory amplitude deduced for the Big Joe flight for the range of time shown.

It should be pointed out that there is considerable uncertainty as to the reliability of the high angle-of-attack cylinder heat-transfer calculations. This uncertainty is due in part to a lack of detailed knowledge of the boundary layer and flow-field conditions over a range of Reynolds numbers at high angle of attack. However, the

angle-of-attack data of figure 8 (which was obtained at $R_{\infty,D} = 1.6 \times 10^6$ compared with the Big Joe value at peak heating of $R_{\infty,D} = 0.98 \times 10^6$) suggest a result similar to that obtained above. It therefore appears that the heating rates experimentally determined at midcylinder thermocouple 12 are greater than would be expected. A possible explanation is given below but further flight data are required to confirm the existence of the high heating rates at station 12.

The fact that the heating rates obtained at thermocouple 11 lie considerably below the turbulent estimates suggests the possibility that laminar flow existed at that station. In this case, a shorter effective length for the turbulent layer should have been used in the theoretical estimate for thermocouple 12. This calculation would have resulted in estimates which were considerably higher than shown, inasmuch as the distance has a powerful influence for small values of the reference length. It should be remembered, however, that the skin-friction relation, as well as the boundary-layer theory itself, is not valid for small distances. Thus, although the high midcylinder heating rates can be qualitatively explained by this concept, it is not quantitatively useful since the theory cannot be made to approach a limit as the distance approaches zero.

G
8

REFERENCES

1. Chapman, Dean R.: A Theoretical Analysis of Heat Transfer in Regions of Separated Flow. NACA TN 3792, 1956.

2. Larson, Howard K.: Heat Transfer in Separated Flows. Rep. No. 59-37, Inst. Aero. Sci., Jan. 1959.

3. Powers, William E., Stetson, Kenneth F., and Adams, Mac C.: A Shock Tube Investigation of Heat Transfer in the Wake of a Hemisphere-Cylinder, With Application to Hypersonic Flight. Rep. No. 59-35, Inst. Aero. Sci., Jan. 26-29, 1959.

4. Pritts, O. R. and Mallard, S. R.: Pressure and Heat Transfer Distribution on a One-Tenth Scale Mercury Capsule at Mach Number 8. AEDC-TN-59-164 (Contract No. AF 40(600)-800), Arnold Eng. Dev. Center, Jan. 1960.

5. Taylor, Nancy L., Hodge, Ward F., and Burbank, Paige B.: Heat-Transfer and Pressure Measurements of a 1/7-Scale Model of a Mercury Capsule at Angles of Attack From 0° to $\pm 20^o$ at Mach Numbers of 3.50 and 4.44. NASA TM X-522, 1961.

6. Everhart, Phillip E., and Bernot, Peter T.: Measurements of the Surface Flows, Heat Transfer, Pressure Distribution, and Longitudinal Stability of the Project Mercury Capsule at Mach 6.9 and 9.6 in the 11-inch Hypersonic Tunnel. NASA TM X-458, 1961.

7. Wallace, A. R., and Swain, W. N.: Static Stability, Heat Transfer, and Pressure Distribution Tests of NASA-McDonnell Mercury Models at Mach Numbers 17 to 21. AEDC-TN-59-157 (Contract No. AF 40(600)-800), Arnold Eng. Dev. Center, Jan. 1960.

8. Stephens, Emily W.: Afterbody Heating Data Obtained From an Atlas-Boosted Mercury Configuration in a Free Body Reentry. NASA TM X-493, 1961.

9. Newlander, Robert A., Taylor, Nancy L., and Pritchard, E. Brian: Pressure Distribution On Two Models of a Project Mercury Capsule for a Mach Number Range of 1.60 to 6.01 and an Angle-of-Attack Range of 0° to 180°. NASA TM X-336, 1960.

10. Ames Research Staff: Equations, Tables, and Charts for Compressible Flow. NACA Rep. 1135, 1953. (Supersedes NACA TN 1428.)

11. Feldman, Saul: Hypersonic Gas Dynamic Charts for Equilibrium Air.
Res. Rep. 40 AVCO Res. Lab., Jan. 1957.

12. Moeckel, W. E., and Weston, Kenneth C.: Composition and
Thermodynamic Properties of Air in Chemical Equilibrium.
NACA TN 4265, 1958.

13. Eckert, E. R. G.: Engineering Relations for Friction and Heat
Transfer to Surfaces in High Velocity Flow. Jour. Aero. Sci.
(Readers' Forum), vol. 22, no. 8, Aug. 1955, pp. 585-587.

G
8

TABLE I.- SUMMARY OF FACILITIES EMPLOYED IN
MERCURY HEAT-TRANSFER TESTS

Facility	M_∞	$R_{\infty,D}$	Model maximum diameter, in.	Reference
AEDC-B tunnel	8.0	0.26×10^6 to 1.6×10^6	7.45	4
Langley Unitary Plan wind tunnel	3.5 and 4.44	2.7×10^6	10.64	5
Langley Mach 5 blow-down jet	4.95	0.3×10^6 to 4.2×10^6	1.75	- - -
Langley 11-inch hypersonic tunnel	9.6	2×10^5	2.22	6
Ames 10- by 14-inch supersonic tunnel	5.0 6.0	6×10^5 2.8×10^5	2.0	- - -
AEDC Hotshot 2	17 to 21	10^5	9.685	7
Ames 2- by 2-inch shock tunnel	4.9 to 5.4	0.22×10^5 to 0.25×10^5	0.5	- - -

G
8

TABLE II.- ADDITIONAL RESULTS AT $\alpha = 0°$

Facility	M_∞	$R_{\infty,D}$	H, Btu/lb	h_l/h_{sp} for —			
				Cone		Cylinder	
				Measured	Calculated	Measured	Calculated
Ames 10- by 14-inch supersonic wind tunnel	5.0	0.6×10^6	160	0.02 to 0.06	$0.052^*\left(\dfrac{l_2}{D} = 0.45\right)$	$0.26\left(\dfrac{l_2}{D} = 0.95\right)$	$\left\{\begin{array}{l}0.074^*\left(\dfrac{l_2}{D} = 0.95\right)\\ .44^{**}\left(\dfrac{l_2}{D} = 0.95\right)\end{array}\right.$
	6.1	$.29\times10^6$	192	.02 to .06	$.049^*\left(\dfrac{l_2}{D} = 0.45\right)$	$.18\left(\dfrac{l_2}{D} = 0.95\right)$	$\left\{\begin{array}{l}.071^*\left(\dfrac{l_2}{D} = 0.95\right)\\ .37^{**}\left(\dfrac{l_2}{D} = 0.95\right)\end{array}\right.$
AEDC Hotshot 2 (Ref. 7)	20.6	$.88\times10^5$	1,600	.006 to .022	———	$.018\left(\dfrac{l_2}{D} = 1.06\right)$	$.022^*\left(\dfrac{l_2}{D} = 1.06\right)$
Ames 2- by 2-inch shock tunnel	4.95 to 5.4	$.22\times10^5$ to $.25\times10^5$	5,100	.013 to .022	———	———	———

*Indicates laminar theory
**Indicates turbulent theory
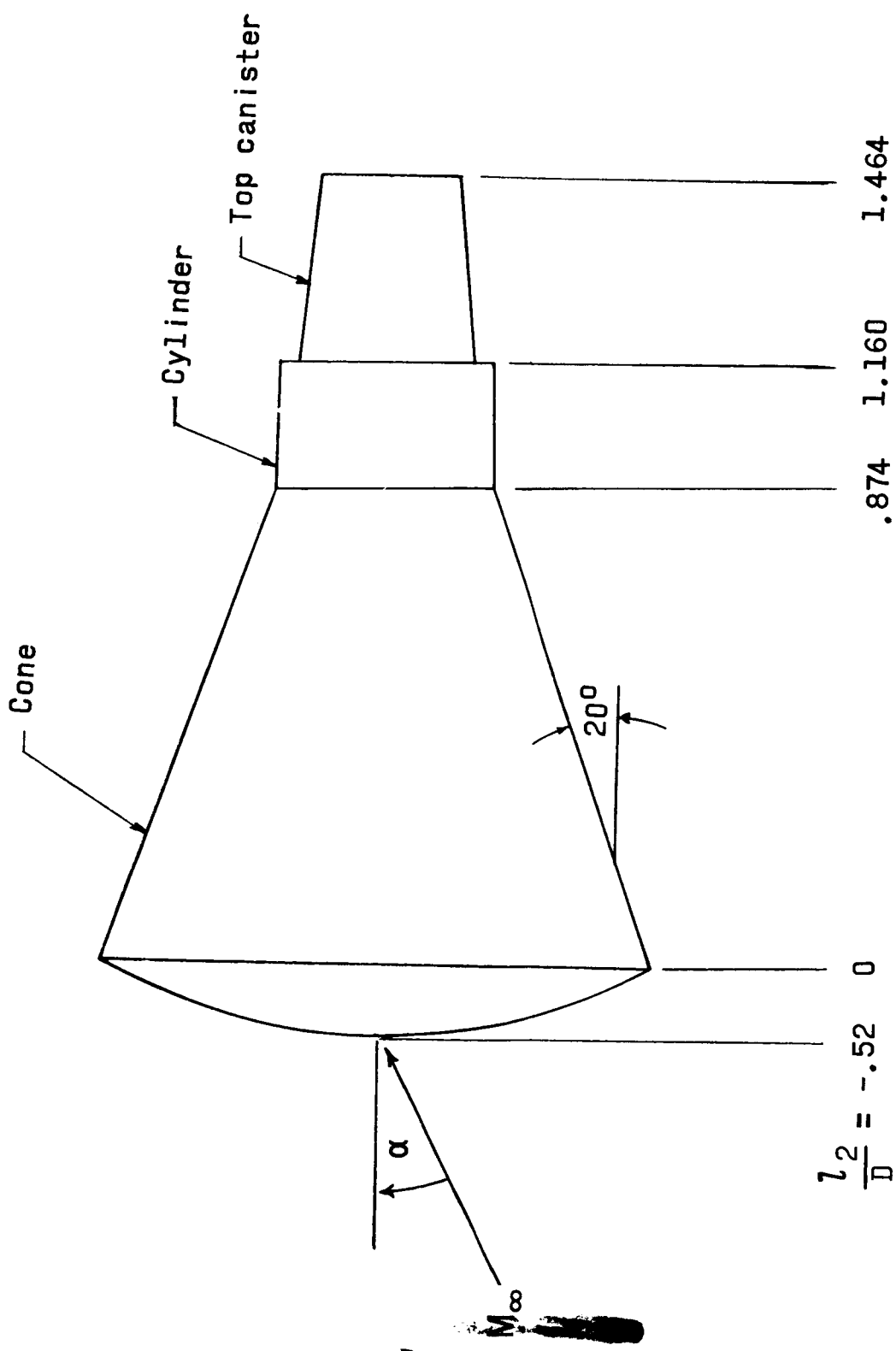
Figure 1.- Mercury reentry configuration.
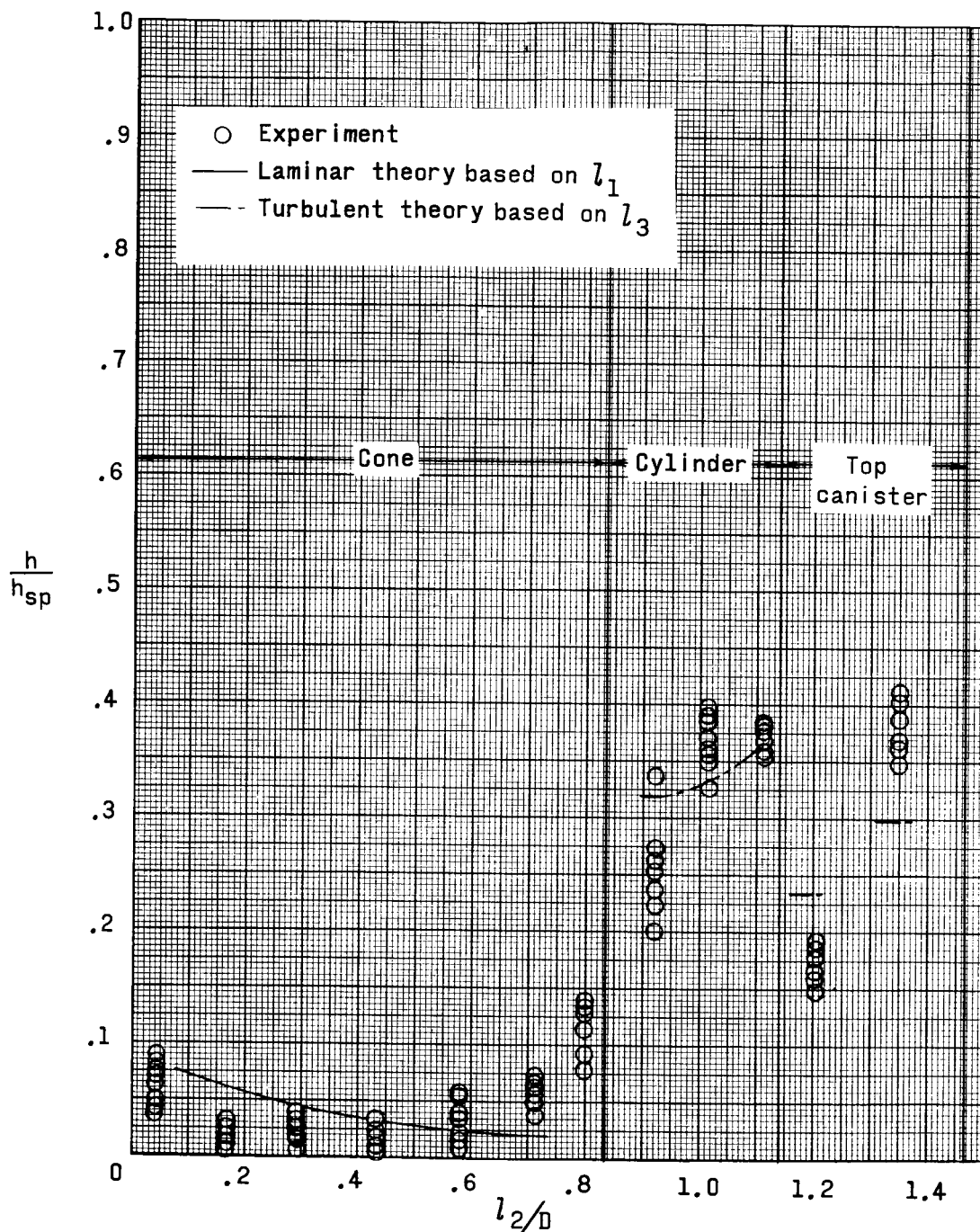
Figure 2.- Afterbody heat-transfer coefficient distribution. $\alpha = 0^{\circ}$; $M_{\infty} = 8$; $R_{\infty,D} = 1.6 \times 10^{6}$.
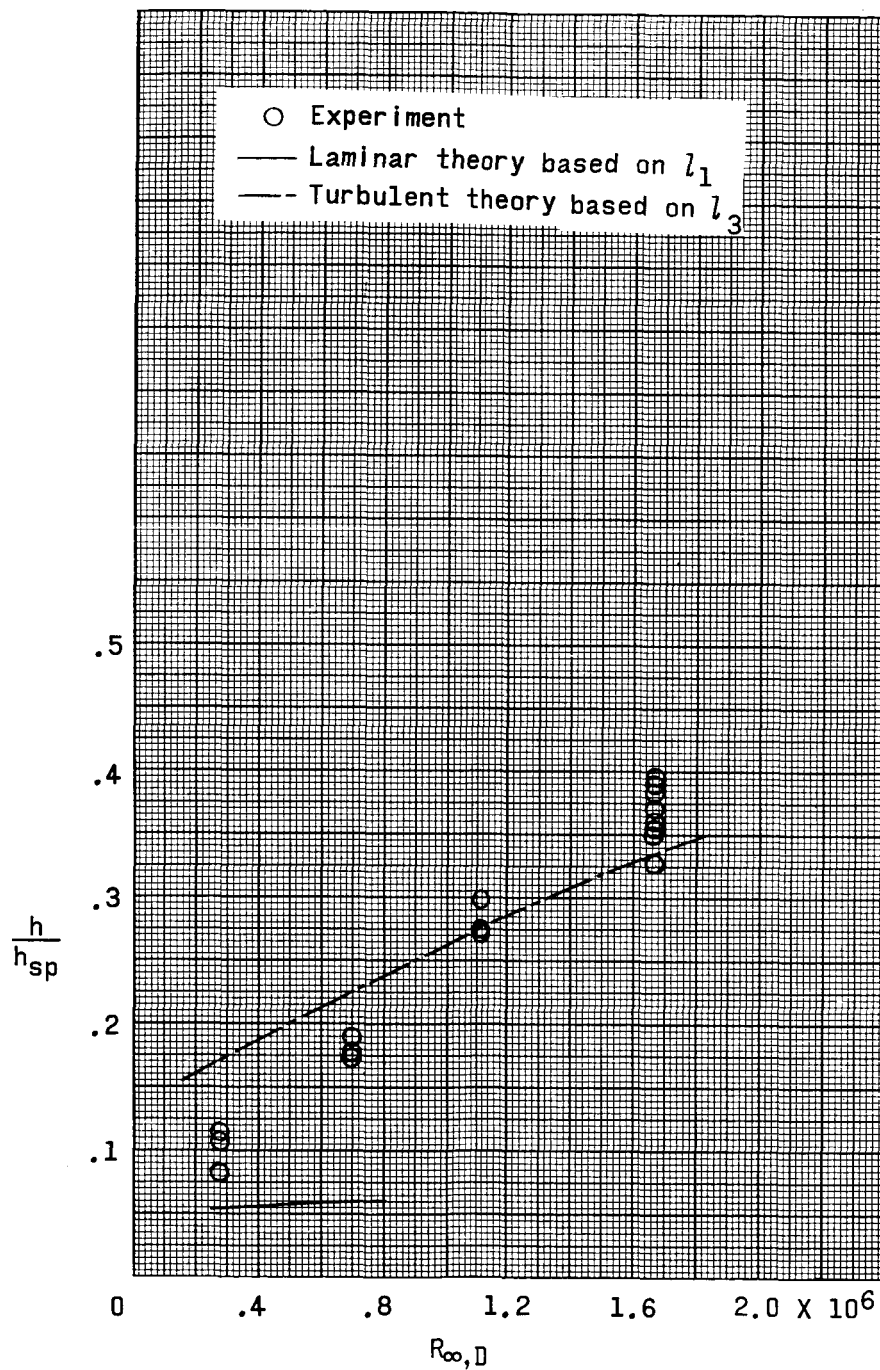
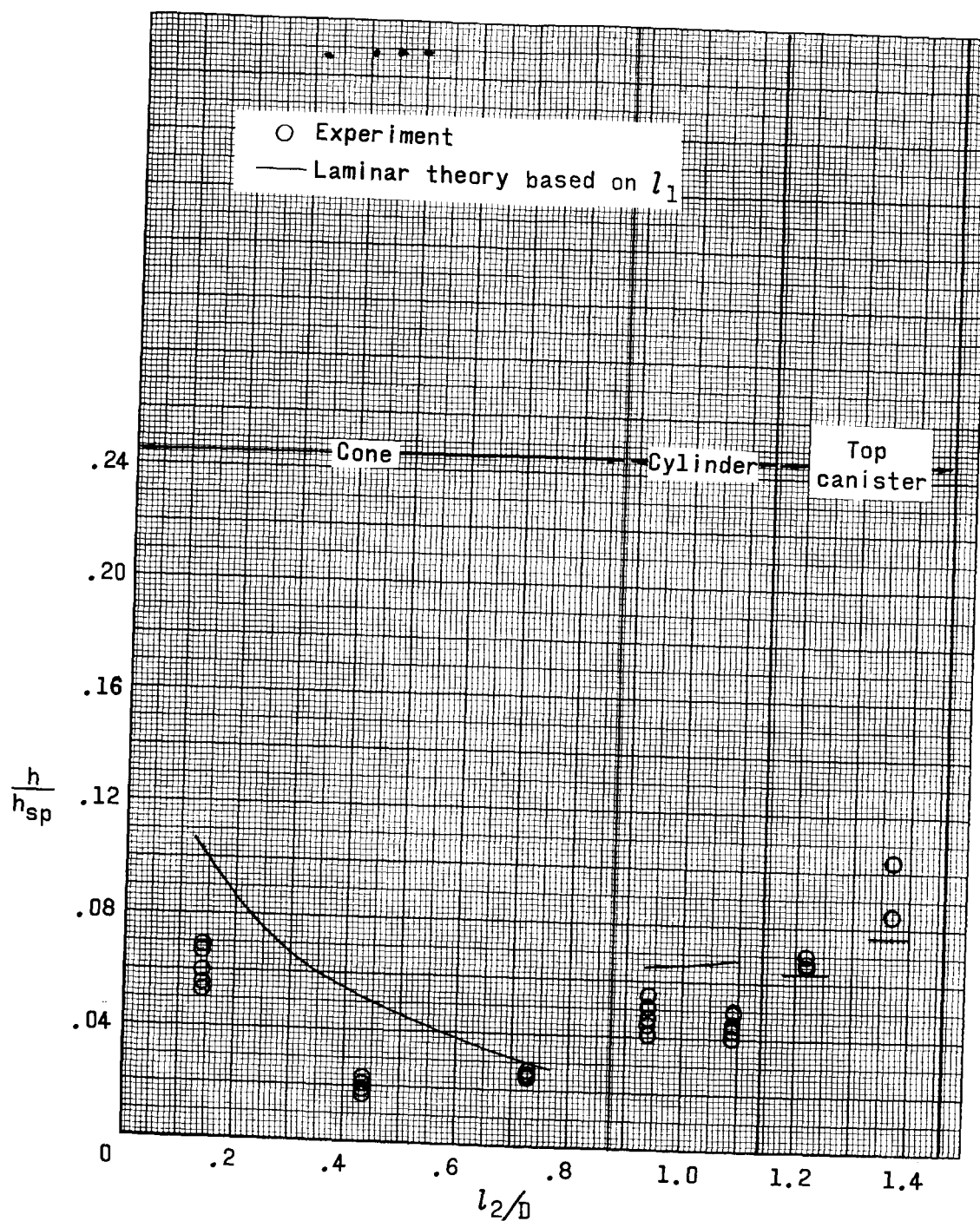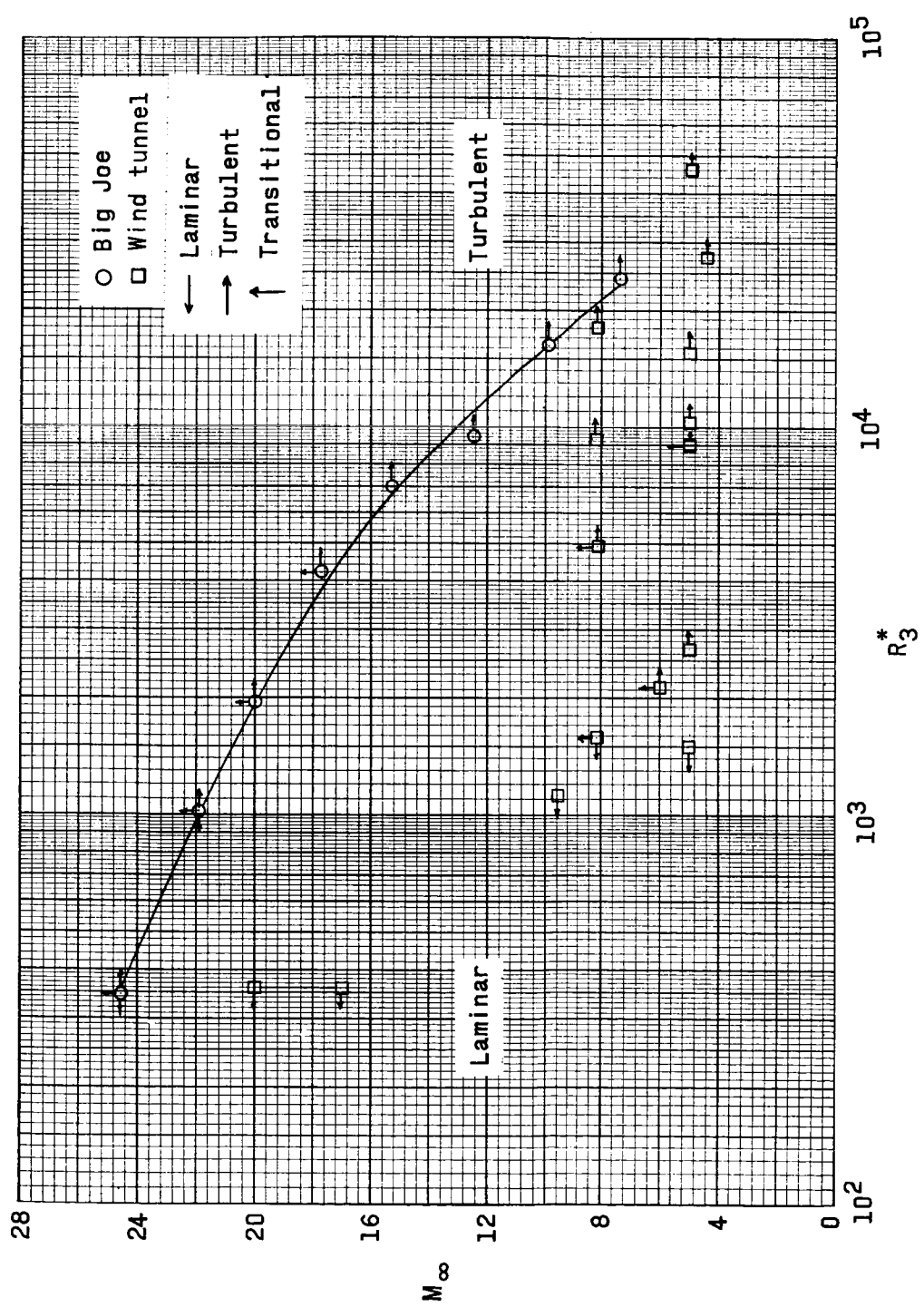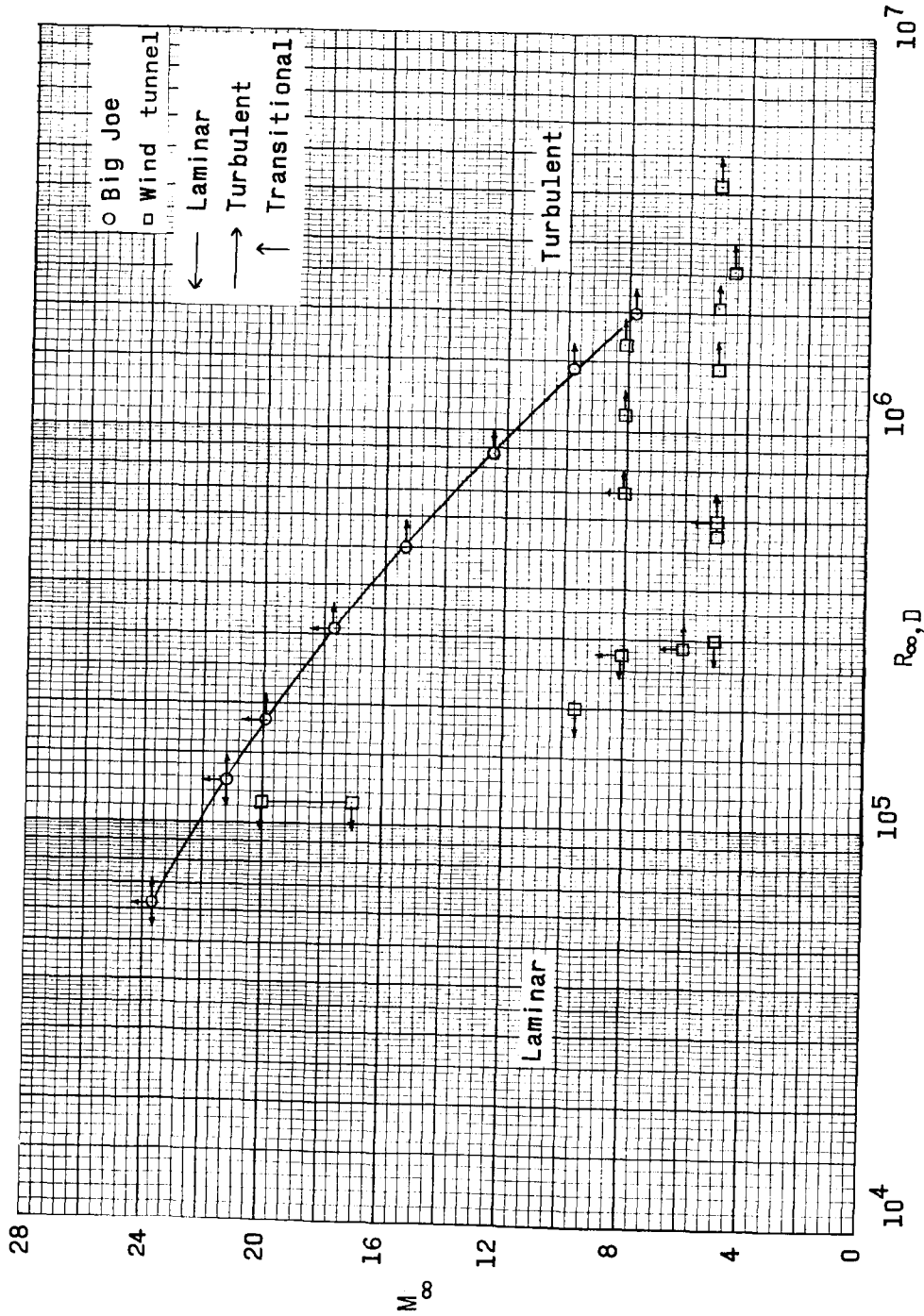Figure 3.- Effect of Reynolds number on midcylinder heat-transfer coefficient. $\alpha = 0°$; $M_\infty = 8$.
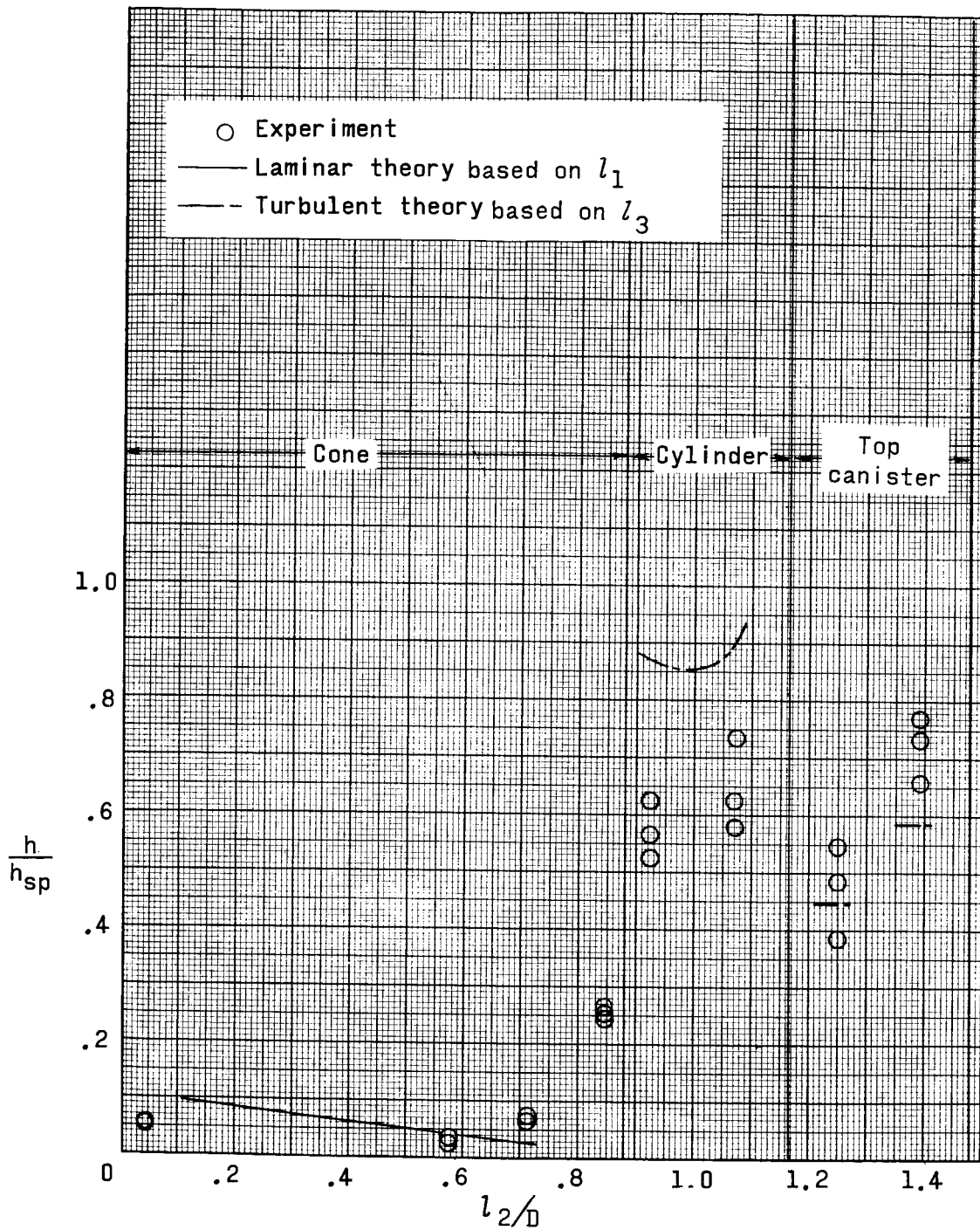
Figure 4.- Afterbody heat-transfer coefficient distribution. $\alpha = 0^\circ$; $M_\infty = 4.44$; $R_{\infty,D} = 2.7 \times 10^6$.
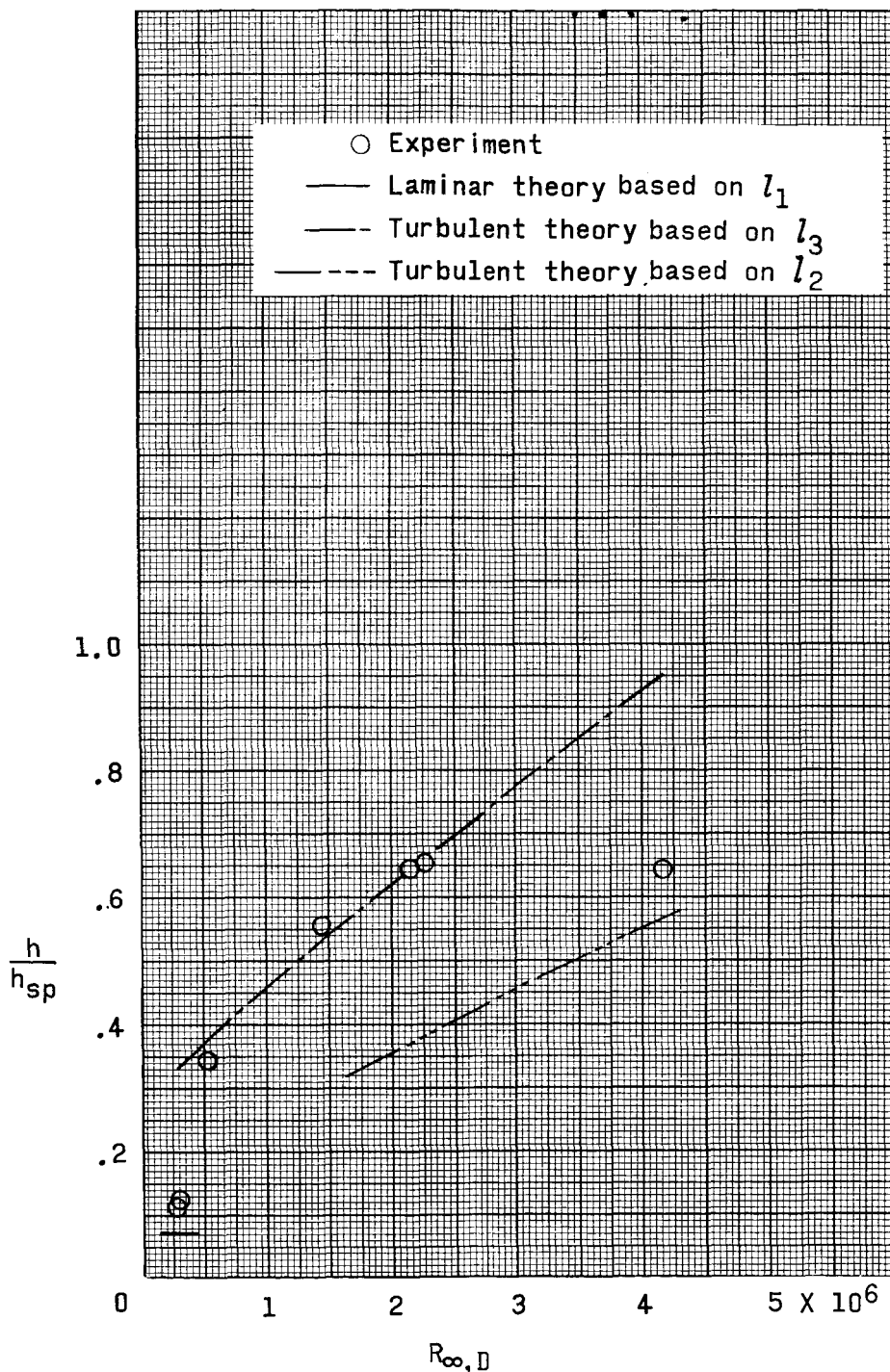
Figure 5.- Effect of Reynolds number on midcylinder heat-transfer coefficient. $\alpha = 0°$; $M_\infty = 4.95$.

Figure 6.- Afterbody heat-transfer coefficient distribution.
$\alpha = 0^{\circ}$; $M_{\infty} = 9.6$; $R_{\infty,D} = 2 \times 10^5$.

(a) Local Reynolds number correlation.

Figure 7.- Condition of boundary layer at midcylinder.

(b) Free-stream Reynolds number correlation.

Figure 7.- Concluded.
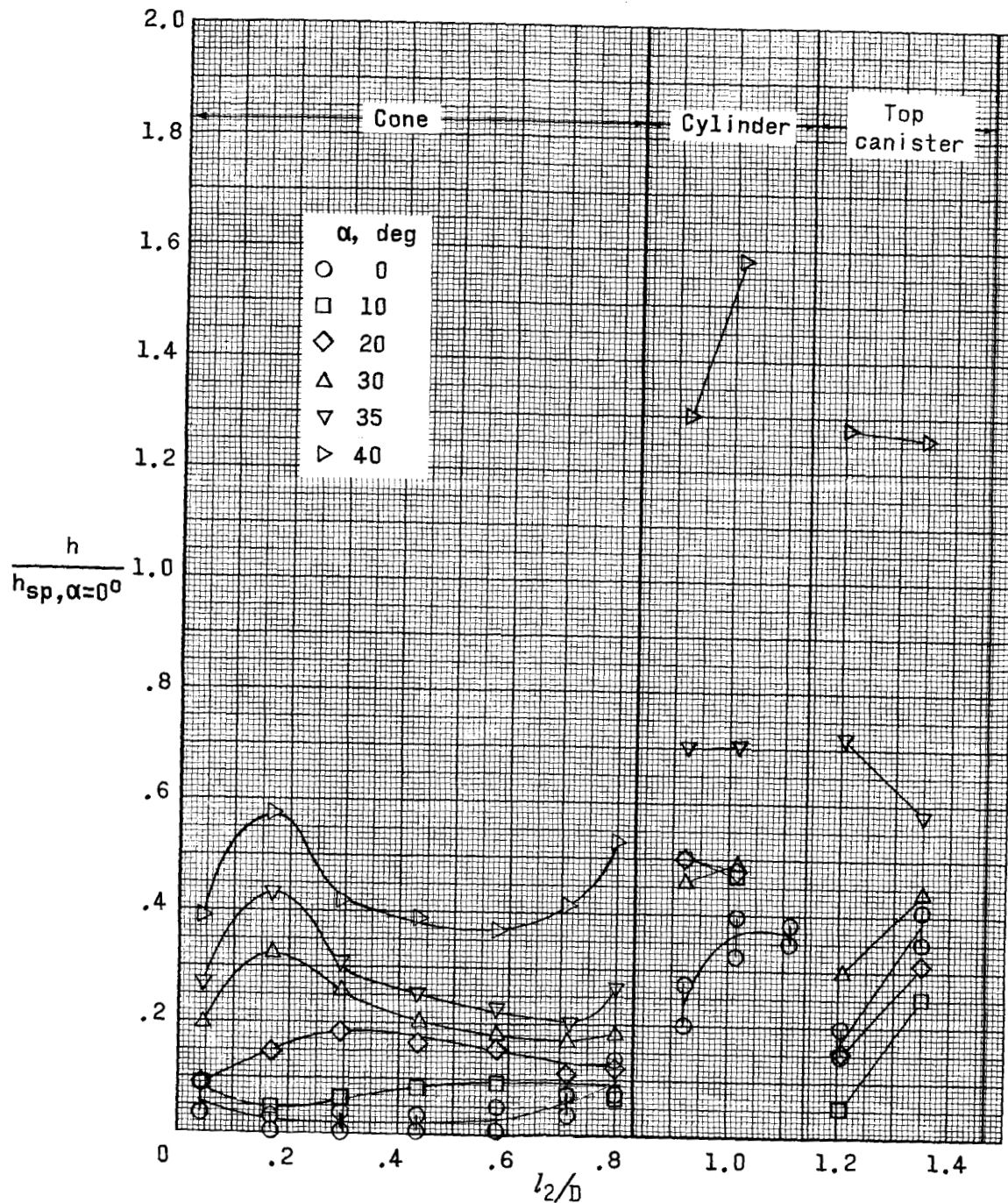
Figure 8.- Effect of angle of attack on heat-transfer coefficient distribution. $M_\infty = 8$; $R_{\infty,D} = 1.6 \times 10^6$.
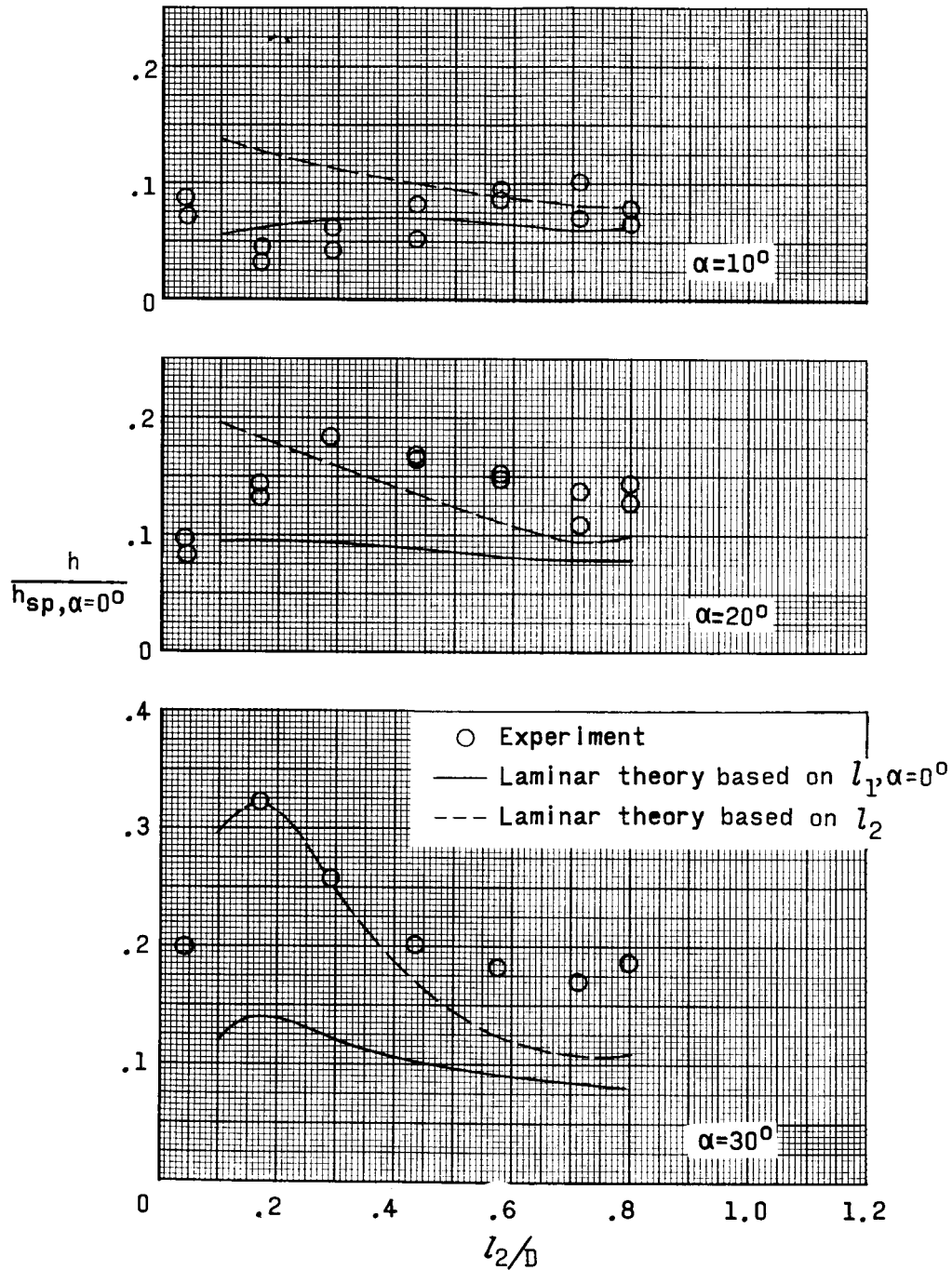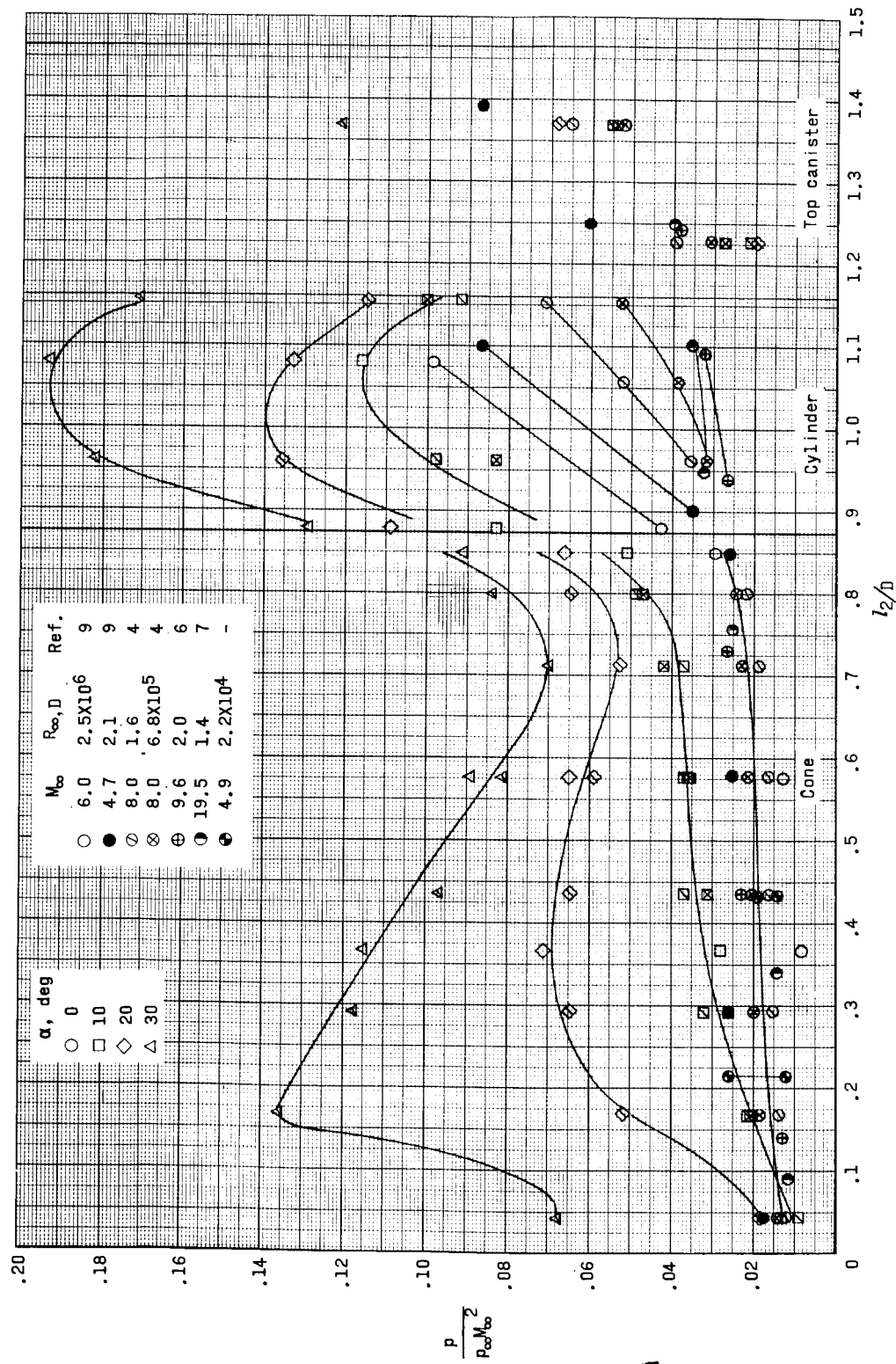
Figure 9.- Effect of angle of attack on conical-section heat-transfer coefficient distribution. $M_\infty = 8$; $R_{\infty,D} = 1.6 \times 10^6$.
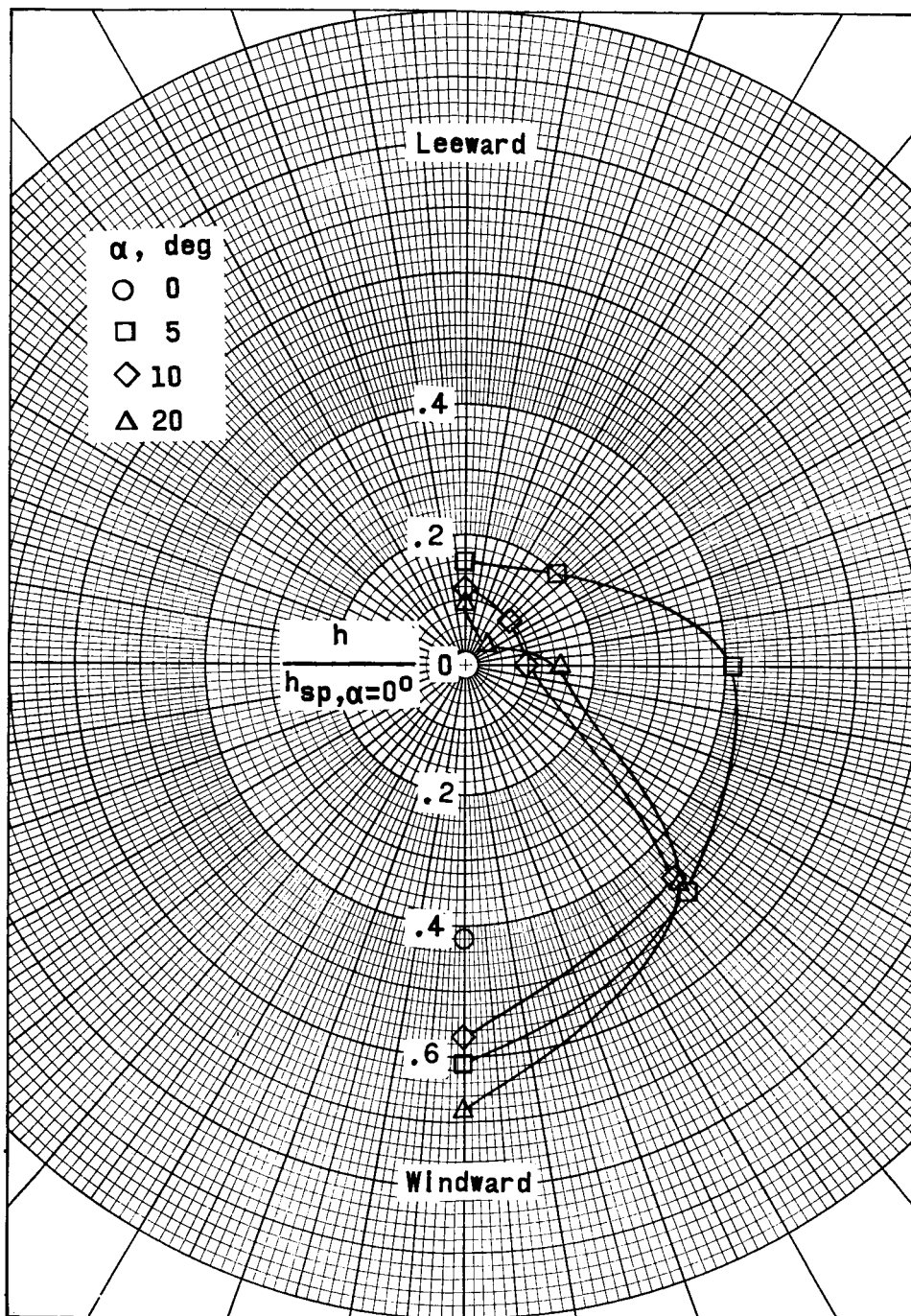
Figure 10.- Effect of angle of attack on midcylinder circum-
ferential heat-transfer coefficient distribution.
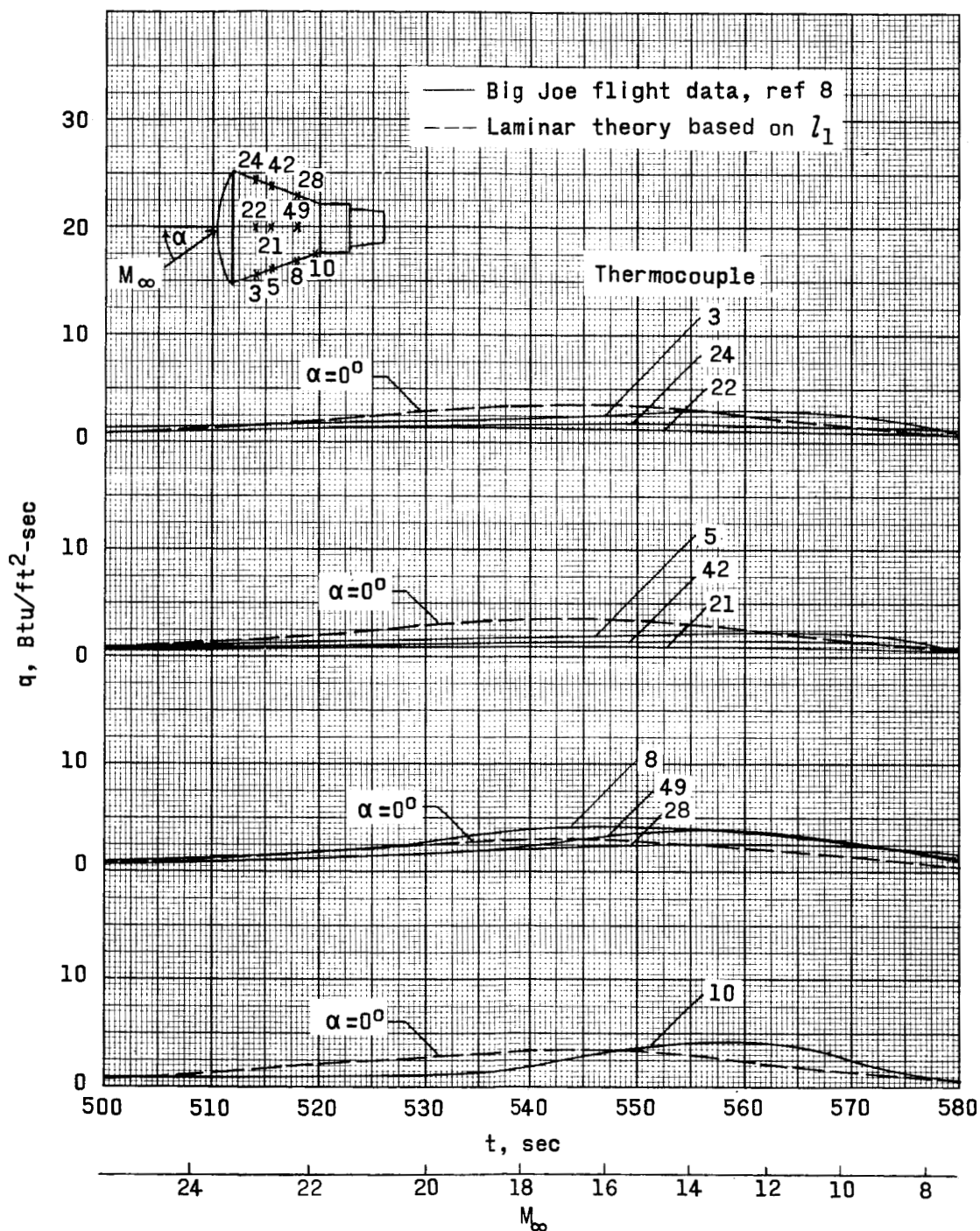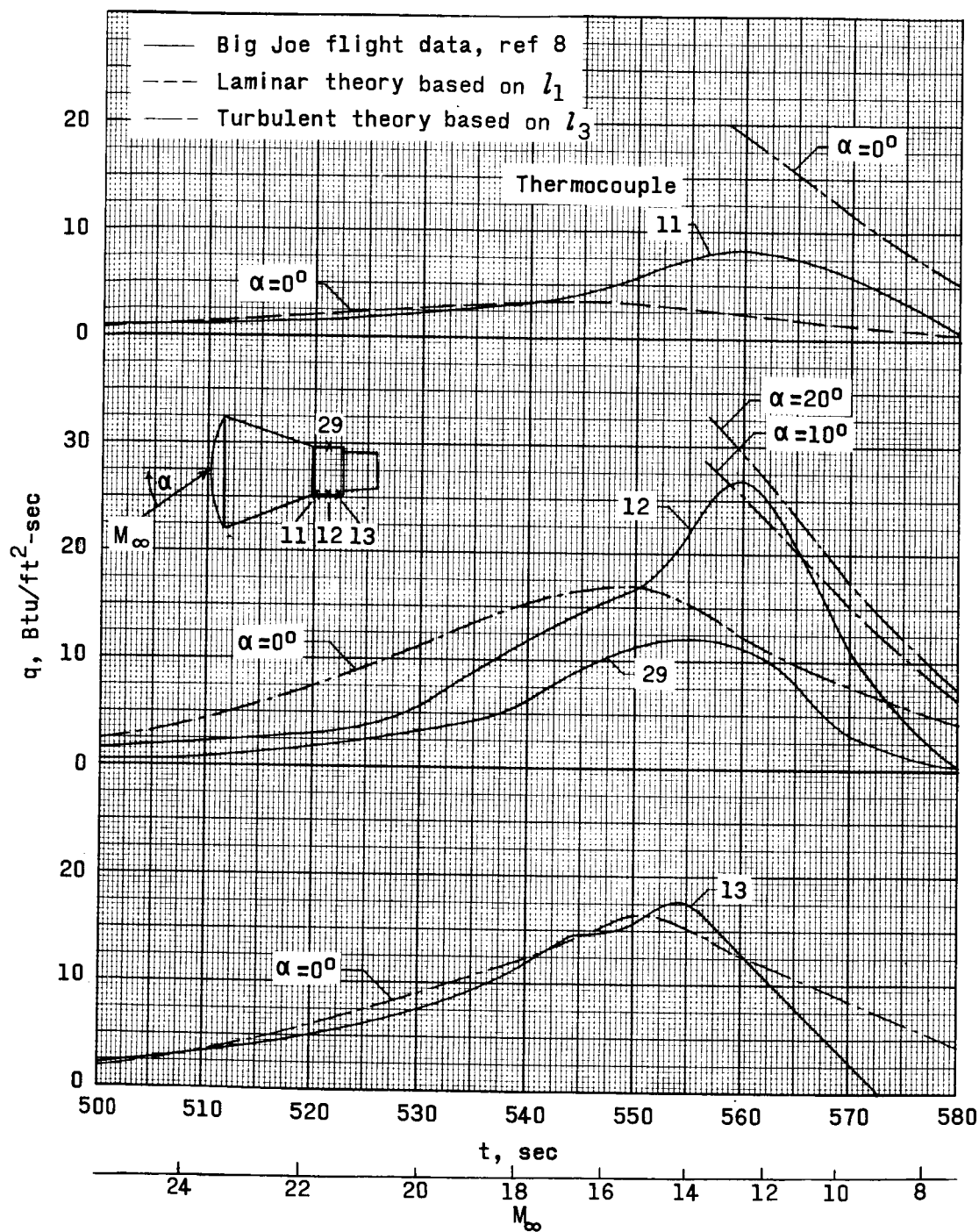$M_\infty = 4.95$; $R_{\infty,D} = 2.1 \times 10^6$.

Figure 11.- Afterbody reentry pressure distribution. Key for Mach number and Reynolds number given for α = 0° applies to all values of α.

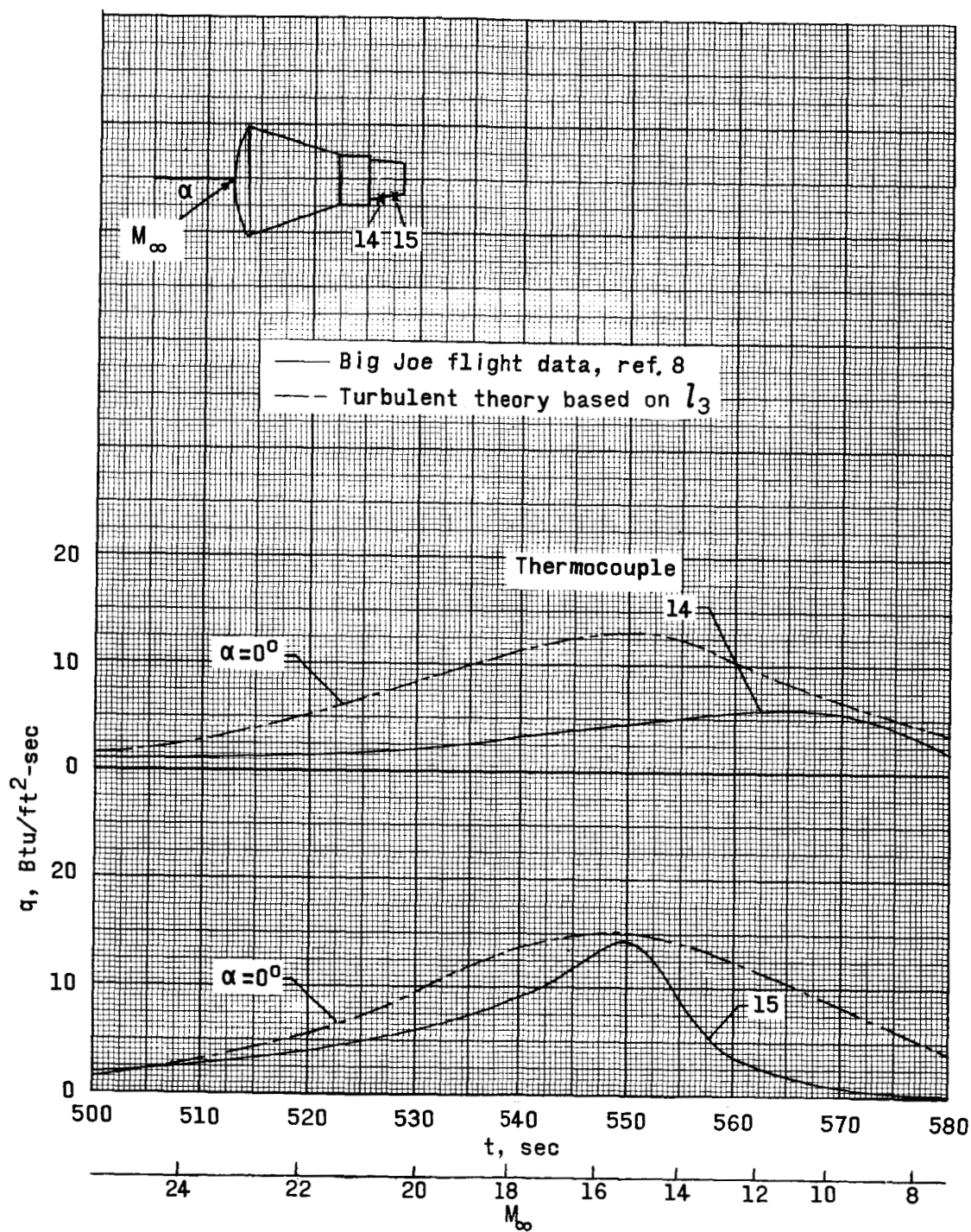(a) Conical section.

Figure 12.- Big Joe heating rate history.

(b) Cylindrical section.

Figure 12.- Continued.

(c) Top canister section.

Figure 12.- Concluded.